Multi-objective shape optimization of a plate heat exchanger: a multi-scale approach

Franck Mastrippolito, Stéphane Aubert, Frédéric Ducros, Martin Ferrand, Jean-François Fourmigué

Multi-objective shape optimization of a plate heat exchanger: a multi-scale approach

Franck Mastrippolito
Univ. Lyon, Ecole Centrale de Lyon
Laboratoire de Mécanique des Fluides et d'Acoustique UMR5509
France

Univ. Grenoble Alpes, CEA, LITEN, DTBH, Laboratoire Echangeurs et Réacteurs
France

franck.mastrippolito@cea.fr

Stéphane Aubert
Univ. Lyon, Ecole Centrale de Lyon
Laboratoire de Mécanique des Fluides et d'Acoustique UMR5509
France
stephane.aubert@ec-lyon.fr

Frédéric Ducros
Univ. Grenoble Alpes, CEA, LITEN, DTBH, Laboratoire Echangeurs et Réacteurs
France
frederic.ducros@cea.fr

Martin Ferrand
MFEE,
EDF R&D
France
martin.ferrand@edf.fr

Jean-François Fourmigue
Univ. Grenoble Alpes, CEA, LITEN, DTBH, Laboratoire Echangeurs et Réacteurs
France
jean-francois.fourmigue@cea.fr

ABSTRACT

This work considers the shape optimization of a crossflow plate heat exchanger air/water. The two objectives are to maximize the effectiveness while minimizing the total pressure drop. The shape variation concerns a trapezoidal rib mounted on the hot channels plates. A multiscale approach is presented, coupling CFD simulations and a NTU method. The optimization method is based on a genetic algorithm and kriging metamodels with adaptive sampling. Infill criteria are the maximum mean square error (*MMSE*) and multi-points expected improvement (*q-EI*). A clustering of the Pareto front individuals highlights a finite number of optimal shapes.

KEYWORDS

Heat exchanger, Multi-objective optimization, CFD, Kriging, adaptive sampling, Self-Organizing Maps

INTRODUCTION

Heat exchangers (HEX) are widely used in many industrial applications as power engineering, chemical industry, transport and spatial. Heat transfer enhancement and heat exchangers design are still investigated in order to improve energy efficiency. Periodic ribs or fins are a common way to achieve an efficient heat transfer enhancement [1,2]. Several numerical and experimental studies have shown that the shape of such obstacles has a strong influence on the aero-thermal behavior [2–4].

Heat exchangers optimization is growing in interest over the past decade. Various studies are interested by the optimization of HEX performances using correlations and integral methods coupled to a genetic algorithm (GA). Selbas et al. [5] use a mono-objective GA to improve the heat transfer area of a shell and tubes HEX. Guo et al. [6] apply a multi-objective genetic algorithm (*NSGA-II*) to minimize the entropy production of a shell and tubes HEX. Sanaye and Hajabdollahi [7] optimize the effectiveness and cost of a shell and tubes HEX using *NSGA-II* and NTU method. A drawback of such methods is the use of correlations which drives the optimum search.

Thus, computational fluid dynamics (CFD) simulations were used to quantify the aerothermal behavior of non-conventional shapes in HEX and to perform optimization [8–12]. The optimization purpose is to maximize the performances of a unique HEX channel expressed using Nusselt number, total pressure losses [10–12], the effectiveness or the total heat flux [8,9]. These approaches can precisely evaluate the influence of the shape variation of the obstacles but the performances analysis of the whole HEX is not addressed.

Only few studies concern the HEX optimization with a multiscale approach coupling CFD and integral method [13,14]. CFD simulations of the obstacles are used to build correlations for the Nusselt number and the pressure loss coefficient. These correlations are employed in a NTU method to evaluate the HEX performances. The HEX optimization is thus performed using a GA.

However when CFD simulations are used conjointly to a GA, numerous time consuming simulations are needed. To

deal with this issue, *metamodels* (or surrogated models) are used [15]. The underlying idea is to build an approximation of a costly simulation response using a limited number of *observations*. This cheaper approximation can then be used by the GA. Several metamodelization methods exist as artificial neural networks [13], response surface modelling [14] and kriging models [10,11]. As mentioned in [15], kriging is well suited to build accurate metamodels of complex physics responses. As the optimization results depend on the metamodel quality, *adaptive sampling* is used to improve the interpolation accuracy [10,11,16–18]. The metamodel is iteratively improved by adding new observations to it. For instance, Saleh et al. [10] and Wen et al. [11] add observations from the region near to the current optimum until the metamodel relative mean square error is greater than a tolerance. However, this method may lead to converge on local optimum and stay trapped here [18].
This work proposes a multi-objective HEX optimization based on a multiscale approach and a genetic algorithm. CFD simulations are used to build correlations for the Nusselt number and head loss coefficient. These correlations are used into a NTU method as presented on Section 1. The correlations are obtained by kriging and adaptive sampling based on maximum mean square error (*MMSE*) and expected improvement (*EI*). The optimization tools are introduced on Section 2. Results and analysis are presented on Section 3.

1 THERMAL MODELLING

This section will present the models used to calculate the performances of a crossflow plate heat exchanger (CPHX) with unmixed fluids. CPHX are constituted by a stack of plates as shown in Figure 1(a). Periodic ribs are placed on each hot channel to enhance heat transfer. Their shape has a major influence on the heat transfer. The chosen rib has a trapezoidal symmetric shape as shown Figure 1(b). It is defined by its height (h_{rib}), base width (E) and top width (e). The canal height (H) and the rib-pitch ($L = 3H$) remain constant. The rib angle (α) is only used for the analysis.

The NTU method [1] is employed to compute the effectiveness ε. The total pressure losses ΔP_{tot} are calculated taking into account both cold and hot channels [1]. The rib influence on the CPHX performances is quantified through the Nusselt number Nu and the head loss coefficient C_f.

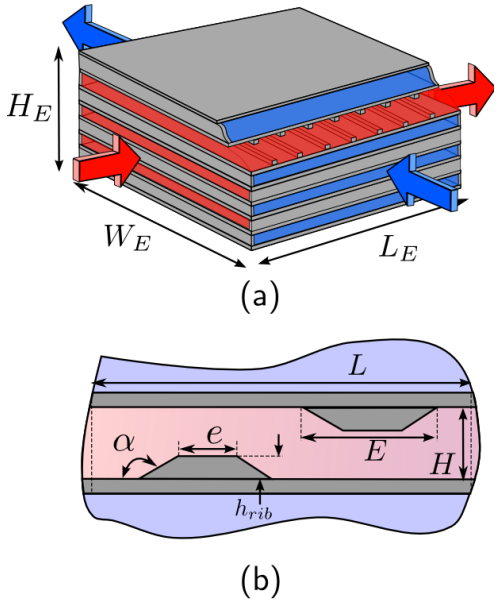

Figure 1: **Schematics of the heat exchanger – (a) Crossflow plate heat exchanger (CPHX) with unmixed fluids – (b) Trapezoidal rib shape parameters.**

1.1 Heat exchanger modelling

The hot stream with $0.56\ kg.s^{-1}$ mass flow rate ($\dot{m}_a$) is air incoming at temperature and pressure of $553.15\ K$ and $300\ kPa$. The cold stream with $2.86\ kg.s^{-1}$ mass flow rate $\dot{m}_w$) is water incoming at temperature and pressure of $353.15\ K$ and $100\ kPa$. The CPHX has 13 hot channels (N_a) and 12 cold ones (N_w). H is set to $7\ mm$ and the plate thickness to $1\ mm$. 20 ribs are mounted on each hot channels. The CPHX dimensions are $H_E = 0.20\ m$ and $W_E = L_E = 0.402\ m$.
The NTU method is presented on Algorithm 1. The Reynolds number Re_{D_H} is based on the hydraulic diameter of a plane channel, $D_H = 2H$.
Dittus-Boelter and Blasius correlations (Algorithm 1 – line 4) and the effectiveness formula of a crossflow unmixed plate heat exchanger (Algorithm 1 – line 9) are from [1].

1.2 Numerical modelling of a periodic rib

Code_Saturne software [19] is used to solve the governing equations for two-dimensional unsteady air flow and heat

Algorithm 1: **CPHX effectiveness and total pressure losses calculation [1]**

Input : $\boldsymbol{p} = (h_{rib}, e, E)$
Input : W_E, L_E, N_a, N_w, H, L
Input : $\{\dot{m}_i\}_{i=a,w}$, $\{T_{in,i}\}_{i=a,w}$, $\{P_{in,i}\}_{i=a,w}$
Output : ϵ et ΔP_{tot}

1 Reference temperature and pressure ($\{T_{ref,i}\}_{i=a,w}$ and $\{P_{ref,i}\}_{i=a,w}$) set to inlet values
2 Compute thermophysical properties (λ, ρ, c_p, μ) and Prandtl number (Pr) for both fluids
3 Compute velocities and Reynolds numbers :

$$i = a, w, \qquad U_{deb,i} = \frac{\dot{m}}{N_i\, W_E H \rho}$$

$$Re_{D_H,i} = \frac{\rho U_{deb,i} D_H}{\mu}$$

4 Compute Nu et C_f from CFD for hot stream :

$$Nu_a = f_{CFD}(\boldsymbol{p}, Re_{D_H}, Pr)$$

$$C_{fa} = f_{CFD}(\boldsymbol{p}, Re_{D_H})$$

from correlations for cold stream :

$$Nu_w = 0.023 Re_{D_H}^{0.8} Pr^{0.4}$$

$$C_{fw} = 0.316 Re_{D_H}^{-0.25}$$

5 Compute the heat capacity rates :

$$C_{min} = min(\dot{m}_a c_{p,a}, \dot{m}_w c_{p,w})$$

$$C_{max} = max(\dot{m}_a c_{p,a}, \dot{m}_w c_{p,w})$$

$$C^* = \frac{C_{min}}{C_{max}}$$

6 Compute the overall heat transfer coefficient K :

$$\frac{1}{K} = \frac{D_H}{Nu_a \lambda_a} + \frac{D_H}{Nu_w \lambda_w}$$

7 Compute the exchange surface $S_{tot} = 2L_E W_E N_a$
8 Compute the number of transfer unit :

$$NTU = \frac{K S_{tot}}{C_{min}}$$

9 Compute the effectiveness :

$$\epsilon = 1 - exp\left[-(1+C^*)NTU\right] \times \left[I_0(2NTU\sqrt{C^*}) + \sqrt{C^*} I_1(2NTU\sqrt{C^*}) - \frac{1-C^*}{C^*} \sum_{n=2}^{\infty} C^{*n/2} I_n(2NTU\sqrt{C^*})\right]$$

where I is the modified Bessel function.
10 Compute the total pressure losses :

$$\Delta P_{tot} = \sum_{i=a,w} \frac{1}{2} C_f \rho_i U_{deb,i}^2 \frac{L_E}{D_H}$$

11 Compute the outlet temperature :

$$T_{out,a} = [-\epsilon\, C_{min}(T_{in,a} - T_{in,w})/\dot{m}_a c_{p,a}] + T_{in,a}$$

$$T_{out,w} = [\epsilon\, C_{min}(T_{in,a} - T_{in,w})/\dot{m}_w c_{p,w}] + T_{in,w}$$

12 **If** $T_{ref,i} \neq 0.5(T_{in,i} - T_{out,i})$, $i = a, w$ **then** $T_{ref,i} = 0.5(T_{in,i} - T_{out,i})$ et go to line **2**
Else :
End

transfer on the rib channel. The $BL - \overline{v^2}/k$ model is used to predict the turbulence [20]. This wall resolved model takes into account the turbulence anisotropy ($\overline{v^2}$) in the wall normal direction. Thus, it is recommended in heat transfer problems with recirculation areas such as ribs [20,21]. The boundary conditions are visible Figure 2. The fluid and solid domains are thermally coupled (blue lines) using a monolithic formulation. An imposed flux density $\dot{q}$ is applied on the plates (red lines). The flow is assumed spatially developed, thus a streamwise periodic condition is applied (green lines).
The mesh is an unstructured grid with about 100 000 cells mixing hexahedral and prismatic elements (see Figure 2). A boundary layer mesh is used to satisfy the $y^+ \leq 1$ condition for the first cell near the wall, required by the model.

The Nusselt number is calculated at the surface $2LW_E$ as:

$$Nu = \frac{Q\, D_H}{\lambda_a\, 2\, L\, W_E \left(T_{wall} - 0.5(T_{in} + T_{out})\right)} \qquad (1)$$

with T_{wall} and Q the mean surface temperature and total heat flux at the bottom ant top walls (red), T_{in} and T_{out} the bulk temperature at the inlet and outlet (green). The solid conduction into the plate is embedded on Nu. The head loss coefficient is calculated as:

$$C_f = \frac{\Delta P_{in,out}}{0.5\, \rho_a U_{deb}^2} \frac{D_H}{L} \qquad (2)$$

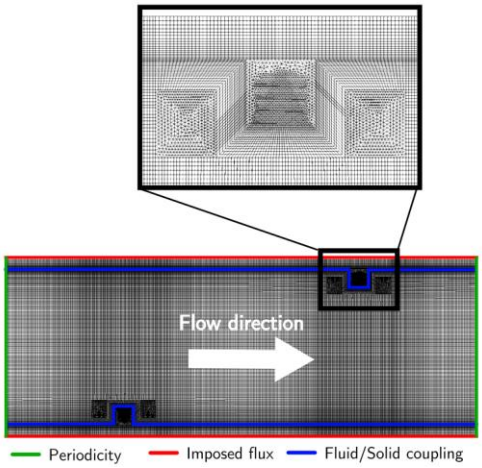

Figure 2: **Numerical Calculation domain, mesh and boundary conditions**

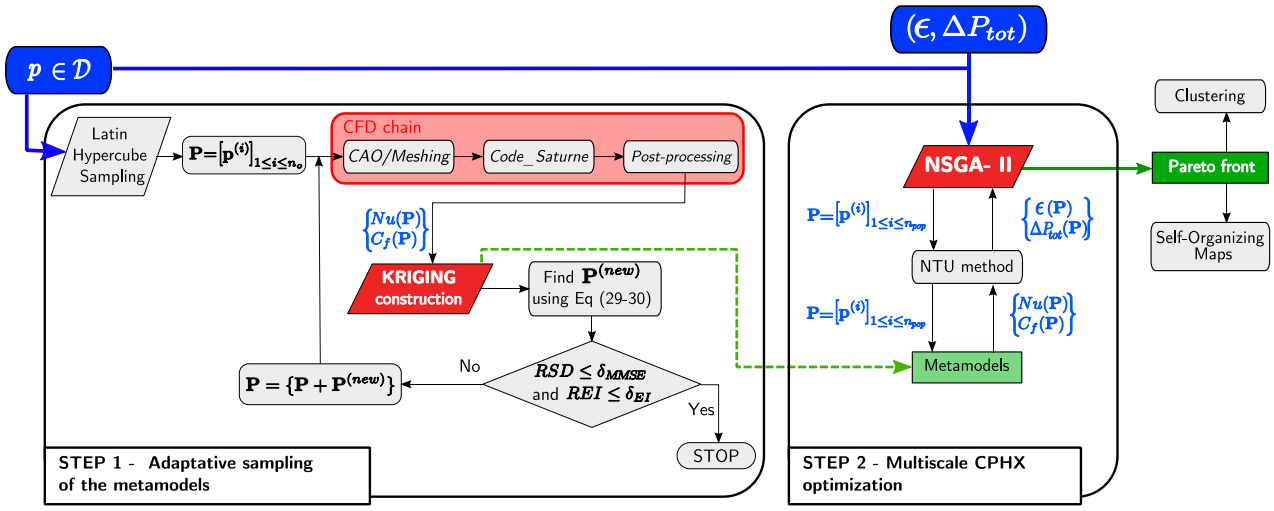

Figure 3: **Flowchart of the optimization process. Step1 is the adaptive sampling building of the metamodels. The Step 2 is the optimization of the CPHX performed with the NSGA-II, NTU method and the correlations of Nu and C_f.**

with $\Delta P_{in,out}$ the pressure drop between inlet and outlet and U_{deb} the bulk velocity.

2 OPTIMIZATION METHOD

The aim of this study is to maximize the CPHX effectiveness ε while minimizing the total pressure losses ΔP_{tot} by varying the rib shape. Formally, the bi-objective problem is written as:

$$\begin{aligned} &\text{maximize} && \varepsilon(\boldsymbol{p}) && (3)\\ &\text{minimize} && \Delta P_{tot}(\boldsymbol{p}) && (4)\\ &\text{with} && \boldsymbol{p} \in \mathcal{D} && (5)\\ &\text{subject to} && h_{rib}/H \in [0.05; 0.3] && (6)\\ & && e/2H \in [0.0375; 0.45] && (7)\\ & && E/2H \in [0.03375; 0.525] && (8)\\ & && E \geq 0.9e && (9) \end{aligned}$$

where $\boldsymbol{p}$ is the vector of parameters and $\mathcal{D} = \{h_{rib}, e, E \mid Eqs.(6-9)\} \subset \mathbb{R}^3$ is the constrained parameters space. The constraint Eq. (9) avoids not manufacturable shapes. $\mathcal{F} = \{\varepsilon, \Delta P_{tot}\}$ is the objective space. The solution of the problem is one or several lines in $\mathcal{F}$, called the *Pareto front*, and represents the best compromise between both objectives. The method used to solve the above problem is presented on Figure 3.

2.1 Motor of optimization – NSGA-II

Motors of optimization are used to solve optimization problems. For mono-objective problems, gradient based or direct search methods are well used [22]. For multi-objectives ones, meta-heuristic methods as genetic algorithms (GA) are preferred [22]. In this study, the genetic algorithm NSGA-II is used [23]. This GA is employed in numerous studies for various domains [9,13,22,24] due to its robustness and its capability to well describe the Pareto front.

Based on Darwinism principles, GAs simulate the evolution of a set of *individuals* gathering into a *population*, over several *generations*. An individual is characterized by a vector of parameters (*genes*) and the values of the objective functions associated (*phenotype*). The basic steps of a genetic algorithm are:

- **Evaluation**: for a given vector of parameters, the objectives function are evaluated. Usually this operations is realized by an external program: the NTU method in this study.
- **Selection**: the fittest individuals are selected. NSGA-II performs this selection using the Pareto dominance relationship [23].
- **Reproduction**: the combination of the genes of the selected individuals (parents) leads to news ones (offsprings).
- **Mutation**: the genes of some random individuals are modified to explore new solutions.

By repeating these steps at each generation, the best individuals breed and bring closer to the Pareto front.

In order to ensure the exploration of the entire parameters space $\mathcal{D}$, the population size is set to 900 individuals over 200 generations in this study. This leads to 18000 evaluations through the NTU method and as much CFD simulations to estimate Nu and C_f, as shown Figure 3 – Step 2. In the state, the numerical resources needed limit the use of the method in an industrial design process. The use of metamodels is thus mandatory [10] to reduce the cost of evaluating the Nusselt number and the head loss coefficient. In order to build versatile metamodels, the rib performances are evaluated on the whole parameters space $\mathcal{D}$ and for a Reynolds number varying from 3000 to 13000. The extended parameters space is then:

$$\mathcal{D}_e = \left\{\mathcal{D} \cup Re_{D_H} \in [3000; 13000]\right\} \subset \mathbb{R}^4 \quad (10)$$

Rib performances are normalized using Dittus-Boelter Nu_0 and Blasius C_{f0} correlations for smooth channels [1]. Minimization is considered for metamodeling, thus the opposite of the Nusselt number is employed. As presented thereafter, metamodels are built using *kriging models*.

2.2 Metamodeling – Kriging theory

Kriging is a geostatistical interpolation method extended by Sacks et al. [25] to the design and analysis of computer experiments. There are several variants of the kriging models [26] and the universal kriging is used in this study.

Kriging treats the deterministic response $y(\boldsymbol{p}) \in \left\{-Nu/Nu_0\,, C_f/C_{f0}\right\}$ as a realization of a random process $Y(\boldsymbol{p})$ defined as:

$$Y(\boldsymbol{p}) = \sum_{i=1}^{n_p} \beta_i d_i(\boldsymbol{p}) + Z(\boldsymbol{p}) \quad (11)$$

where $d_i(.)$ are linearly independent known functions (trends) and $Z(.)$ is a stationary random Gaussian process. $Z(.)$ has a mean zero and a stationary covariance kernel defined as:

$$Cov\left(Z(\boldsymbol{p}^{(1)}), Z(\boldsymbol{p}^{(2)})\right) = \sigma^2 R(\boldsymbol{p}^{(1)}, \boldsymbol{p}^{(2)}) \quad (12)$$

σ^2 is the process variance and $R(.)$ is the spatial correlation function which depends on the Euclidean distance between two vectors of parameters $\boldsymbol{p}^{(1)}$ and $\boldsymbol{p}^{(2)}$. Using the Matérn 5/2 covariance kernel, the correlation function for $\boldsymbol{p} \in \mathcal{D}_e$ is:

$$R(\boldsymbol{p}^{(1)}, \boldsymbol{p}^{(2)}) = \prod_{k=1}^{4} \left(1 + \frac{\sqrt{5}\left|p_k^{(1)} - p_k^{(2)}\right|}{\theta_k} + \frac{5\left|p_k^{(1)} - p_k^{(2)}\right|^2}{3\theta_k^{\,2}}\right) \exp\left(\frac{-\sqrt{5}\left|p_k^{(1)} - p_k^{(2)}\right|}{\theta_k}\right) \quad (13)$$

where θ_k is the characteristic length-scales along each parameters[1]. In this study, the trend is defined using $n_p = 5$ linear functions:

$$\sum_{i=1}^{5} \beta_i d_i(\boldsymbol{p}) = \beta_1 + \beta_2 p_1 + \beta_3 p_2 + \beta_4 p_3 + \beta_5 p_4 \quad (14)$$

In order to build the metamodel, a design of experiments (DOE) $\boldsymbol{P}$ is necessary to estimate the kriging parameters. Thus n_o observations of the function y are performed for distinct vectors of parameters $\boldsymbol{p}^{(i)}$:

$$\boldsymbol{P} = \left[\,\boldsymbol{p}^{(i)}\right]_{1 \le i \le n_o} \quad (15)$$

$$\boldsymbol{Y} = y(\boldsymbol{P}) = \left[\,y\left(\boldsymbol{p}^{(i)}\right)\right]_{1 \le i \le n_o} \quad (16)$$

Under these hypothesis, the best linear unbiased predictor for $Y(\boldsymbol{p})$ knowing $\boldsymbol{Y}$, is defined by the kriging mean m_K as [26]:

$$m_K(\boldsymbol{p}) = \boldsymbol{d}(\boldsymbol{p})^T \boldsymbol{\beta} + \boldsymbol{r}(\boldsymbol{p})^T \boldsymbol{R}^{-1}(\boldsymbol{Y} - \boldsymbol{D}\boldsymbol{\beta}) \quad (17)$$

where:

$$\boldsymbol{d}(\boldsymbol{p}) = [d_i(\boldsymbol{p})]_{1 \le i \le n_p} \quad (18)$$

is the vector of basis functions,

$$\boldsymbol{D} = \left[d_j\left(\boldsymbol{p}^{(i)}\right)\right]_{1 \le i \le n_o, 1 \le j \le n_p} \quad (19)$$

is the experimental matrix,

$$\boldsymbol{\beta} = \left[\beta_j\right]_{1 \le j \le n_p} \quad (20)$$

is the vector of generalized least square estimates of β,

$$\boldsymbol{r}(\boldsymbol{p}) = \left[R\left(\boldsymbol{p}, \boldsymbol{p}^{(i)}\right)\right]_{1 \le i \le n_o} \quad (21)$$

is the vector of covariance and

$$\boldsymbol{R} = \left[R\left(\boldsymbol{p}^{(i)}, \boldsymbol{p}^{(j)}\right)\right]_{1 \le i \le n_o, 1 \le j \le n_o} \quad (22)$$

is the covariance matrix.

The kriging parameters $\boldsymbol{\beta}$, σ^2 and $\boldsymbol{\theta} = [\theta_k]_{1 \le k \le 4}$ are estimated so as to maximize the likelihood function defined as [27]:

[1] with $p_1 = h_{rib}$, $p_2 = e$, $p_3 = E$ and $p_4 = Re_{D_H}$

$$Ln(\boldsymbol{\beta},\, \sigma^2, \boldsymbol{\theta}) = -\frac{1}{2}\,(n_o\,(\ln(\sigma^2) + \ln(2\pi) + 1) + \ln(|\boldsymbol{R}|)) \quad (23)$$

$\boldsymbol{\beta}$ and σ^2 are given in closed form as:

$$\boldsymbol{\beta} = (\boldsymbol{D}^T\boldsymbol{R}^{-1}\boldsymbol{D})^{-1}\boldsymbol{D}^T\boldsymbol{R}^{-1}\boldsymbol{Y} \quad (24)$$

$$\sigma^2 = \frac{1}{n_o}(\boldsymbol{Y} - \boldsymbol{D}\boldsymbol{\beta})^T\boldsymbol{R}^{-1}(\boldsymbol{Y} - \boldsymbol{D}\boldsymbol{\beta}) \quad (25)$$

and

$$\boldsymbol{\theta} = \underset{\boldsymbol{\theta}}{\operatorname{argmax}}\ Ln(\boldsymbol{\beta},\, \sigma^2, \boldsymbol{\theta}) \quad (26)$$

Finally, the determinist response $y(\boldsymbol{p}) \in \{-Nu/Nu_0\,, C_f/C_{f0}\}$ is given by:

$$y(\boldsymbol{p}) = m_K(\boldsymbol{p}) \quad (27)$$

Moreover, the kriging model gives an estimation of the accuracy of the prediction at an untried vector of parameters $\boldsymbol{p}$ through the mean square error s_K^2, given as:

$$s_K^2(\boldsymbol{p}) = \sigma^2\left(1 - [\boldsymbol{d}(\boldsymbol{p})^T \quad \boldsymbol{r}(\boldsymbol{p})^T]\begin{bmatrix}0 & \boldsymbol{D}^T\\ \boldsymbol{D} & \boldsymbol{R}\end{bmatrix}^{-1}\begin{bmatrix}\boldsymbol{d}(\boldsymbol{p})\\ \boldsymbol{r}(\boldsymbol{p})\end{bmatrix}\right) \quad (28)$$

2.3 Metamodeling - Adaptive sampling

For the purpose of building cheaper and accurate metamodels, *adaptive sampling* is used [16,17]. Starting from an initial coarse DOE, new vectors of parameters $\boldsymbol{p}^{(new)}$ are iteratively added to the metamodel in order to improve the current optimal area (exploitation) or the global accuracy (exploration). In this study maximum mean square error (*MMSE*) and multipoint expected improvement (*q-EI*) criteria are used [26] to improve both exploration and exploitation. In this study, metamodels are used to build correlations, thus they have to be accurate in the whole parameters space $\mathcal{D}_e$. Moreover, optimum values in Nusselt number and head loss coefficient are correlated to the CPHX performances optimum. Thus it is interesting to build accurate metamodels also in the optimum area.

The basic idea of expected improvement (*EI*) is to add to the metamodel the vector of parameters $\boldsymbol{p}^{(new)}$ which leads to an improvement of the current minimum of $m_K(\boldsymbol{p})$. Thus the *q-EI* criterion adds to the DOE $\boldsymbol{P}$ a set of vectors $\boldsymbol{P}^{(new)} = \left[\boldsymbol{p}^{(i)}\right]_{1\le i\le q}$ which maximizes the improvement [26]:

$$\boldsymbol{P}^{(new)} = \underset{\boldsymbol{P}\in\,\mathcal{D}_e^q}{\operatorname{argmax}}\ \mathbb{E}\left[\min(\boldsymbol{Y}) - \min\left(m_K\left(\boldsymbol{P}^{(new)}\right)\right)\right] \quad (29)$$

with $\mathbb{E}[.]$ the mathematical expectation. Using *q-EI* instead of the standard *EI* allows parallel evaluations of the response y, which is very interesting for costly simulations like CFD ones [26].

The *MMSE* criterion adds to the metamodel the vector of parameters which maximizes the mean square error:

$$\boldsymbol{p}^{(new)} = \underset{\boldsymbol{p}\in\mathcal{D}_e}{\operatorname{argmax}}\ s_K^2(\boldsymbol{p}) \quad (30)$$

In contrary to *q-EI*, *MMSE* is sequential. To permit parallel evaluations, a Kriging Believer like method [28] is applied using *MMSE*.

Step 1 in Figure 3 shows the adaptive sampling of the metamodels. First, the initial DOE $\boldsymbol{P}$ is obtained using an optimized Latin Hypercube Sampling (LHS) based on the centered L^2 discrepancy criteria and performed with the Enhanced Stochastic Evolutionary algorithm [29]. Then, the CFD chain evaluates Nu and C_f and the two metamodels are built using Eq. (17). Thus using Eqs. (29-30), a set $\boldsymbol{P}^{(new)} = \left[\boldsymbol{p}^{(i)}\right]_{1\le i\le q}$ of vectors of parameters is selected to improve each metamodels. These new vectors of parameters are evaluated by the CFD chain and the kriging is computed again. As this process is iterative, stopping conditions are necessary for both criteria. According to Huang [30], the chosen conditions are not concerned by magnitudes issues due to their normalization by the variation range of the known observations:

$$RSD = \frac{\max_{\boldsymbol{p}\in\mathcal{D}_e} s_K^2(\boldsymbol{p})}{\max(\boldsymbol{Y}) - \min(\boldsymbol{Y})} \le \delta_{SD} \quad (31)$$

$$REI = \frac{\max_{\boldsymbol{P}\in\mathcal{D}_e^q} E\left[\min(\boldsymbol{Y}) - \min\left(m_K\left(\boldsymbol{P}^{(new)}\right)\right)\right]}{\max(\boldsymbol{Y}) - \min(\boldsymbol{Y})} \le \delta_{EI} \quad (32)$$

When the two relative tolerances are achieved, the adaptive sampling stop and the metamodels are used into the Step 2.

2.4 Shape modifications

The shape modifications were performed using a parametrized CAO and a robust re-meshing strategy.

2.5 Data analysis

The use of a meta-heuristic method as motor of optimization produces an amount of data which is difficult to analyze using conventional methods. In our case, it is not possible to represent the variations of one objective function over the three parameters using 3D plot. Moreover, it is difficult to

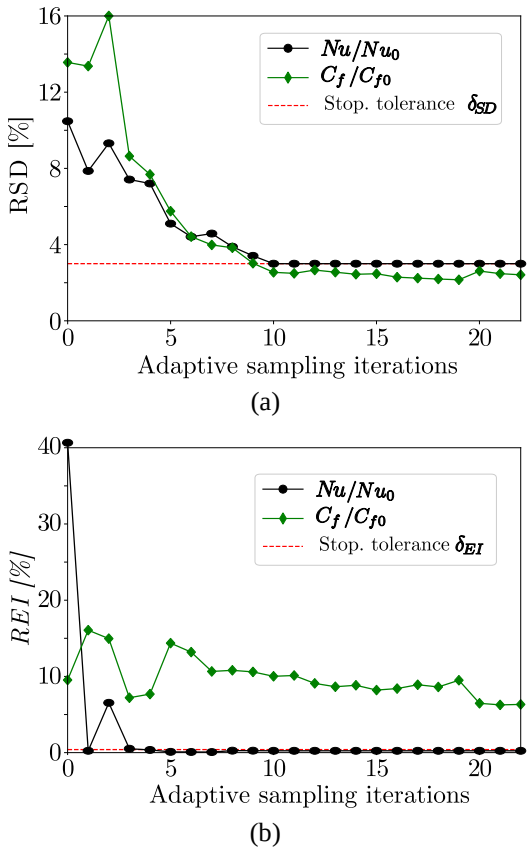

Figure 4: **Convergence history of adaptive sampling conditions for Nu/Nu_0 (black) and C_f/C_{f0} (green) - (a) RSD - (b) REI.**

analyze each shape of the 900 individuals forming the Pareto front.

In order to highlight representative shapes among the Pareto Front, a clustering method is used. Therefore, the solutions are gathered into clusters defined by their centers. The *k-means* clustering proposed by Lee and Kim [31] was found inefficient in this study. Thus, Gaussian mixture based clustering is employed [32].

The results are also visualized using Self-Organizing Maps (SOM) [22]. SOM are artificial neural networks trained using unsupervised learning. Data are represented as a set of maps, each one carrying an information. SOM can be read as geographic maps: the color changes with the information, but one point is rigorously at the same position on every maps. The interdependence between parameters and objectives can be easily observed such as the optimal shapes and performances.

3 Results

3.1 Adaptive sampling convergence

The initial DOE is obtained by an optimized LHS with $n_o = 40$ observations. At each iteration, six vectors of parameters are added to this DOE, two by using *MMSE* and four by using *q-EI*. The tolerances are set to $\delta_{SD} = 3\%$ and $\delta_{EI} = 0.4\%$. The Nusselt number metamodel is based on 48 observations and the pressure loss coefficient one is built using 139 observations.

Figure 4 shows the convergence of the two stopping conditions for both metamodels. As shown Figure 4(a), the

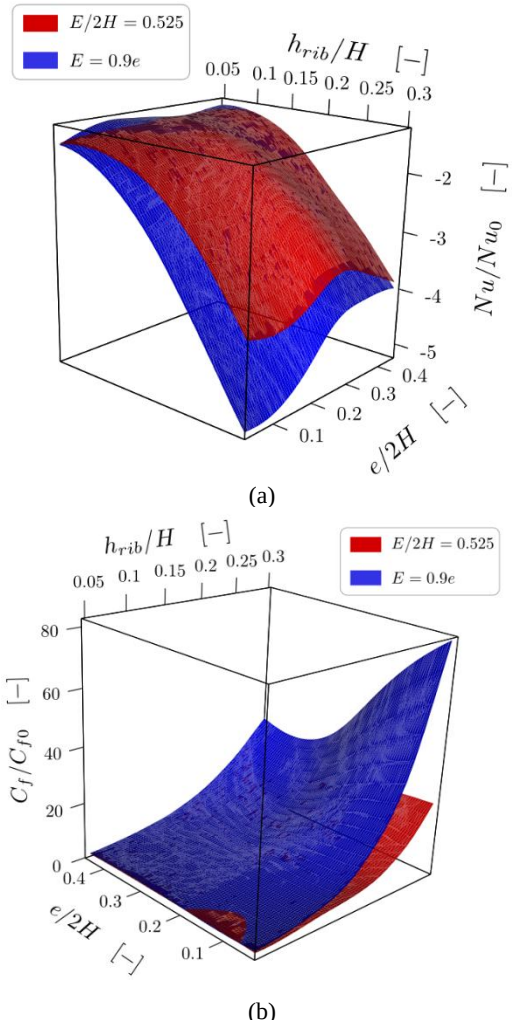

Figure 5: **Response surfaces for Nu/Nu_0 (a) and C_f/C_{f0} (b) over h_{rib}/H and $e/2H$. Re_{D_H} is set to 8000. Two rib base widths are considered: $E = 0.9e$ (blue) and $E/2H = 0.525$ (red)**

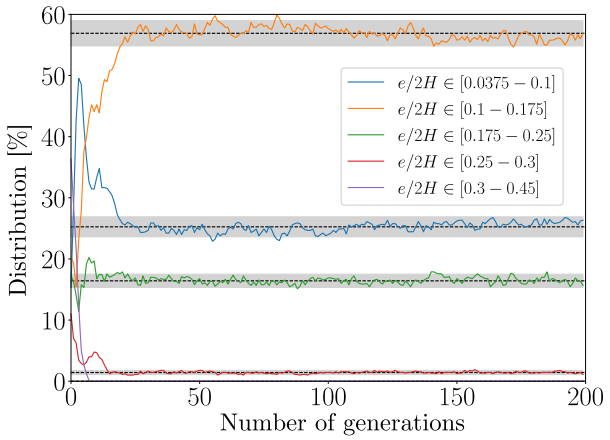

Figure 6: **Evolution of the distribution of the individuals into five classes over the number of generations. Dashed lines represent the mean distribution and grey areas are the 95 %confident bounds.**

condition RSD is reached in 10 iterations for both metamodels. As mentioned by Sasena [16], the *MMSE* criterion gives only a local information about the minimum of likelihood of the metamodel. Thus numerous observations are necessary to obtain a global accurate metamodel. Moreover, it was found that the majority of observations added by *MMSE* are located at the boundaries of the parameters space $\mathcal{D}_e$. It would be interesting of using the integrated mean square error (*IMSE*) [33] criterion instead of the MMSE to add vectors of parameters which improve the global and not only local metamodel accuracy.

Figure 4(b) shows that the condition on the *q-EI* is reached in 4 iterations for $Nu\ /Nu_0$ but is not achieved for $C_f\ /C_{f0}$. The adaptive sampling was thus stopped arbitrarily as the RSD was attained and no major improvement was found in the last iterations for REI.

Figure 5 shows the kriging response surface of the normalized opposite Nusselt number and the normalized head loss coefficient over the height and top width of the rib, for $Re_{D_H} = 8000$ and for two values of $E/2H$.

As shown Figure 5(a), the surface slope around the minimum of $(-\ Nu\ /Nu_0)$ is important. So the *q-EI* criterion locates this area efficiently. On the contrary, as highlighted on Figure 5(b), the minimum area for the head loss coefficient is extended (around $h/H \in [0.05, ; 0.1]$) with a minor surface slope. Thereby, *q-EI* cannot easily converged and adding more points may increase the noise and degrade the interpolation accuracy.

As noticed by these results, the definition of stopping criteria is an open and complex problem [33]. Another approach is to define a budget (in terms of number of simulations or available calculation time) which limits the number of possible observations for the metamodels construction [17].

3.2 NSGA-II convergence

The convergence of the Step 2 is also addressed. A common way to verify this convergence is to look the stability of the Pareto front over the generations [22]. However, the variations of the parameters distribution on $\mathcal{D}$ is also interesting to ensure the convergence of the optimal shapes. This is verified by considering the distribution of the individuals of the Pareto front into several classes of the parameters values, over the generations. Figure 6 shows the individuals distribution into five classes of the top width of the rib. As seen, the distribution does not change after the 30th generation. The 95% confident bounds (grey) are less than 2% of the mean value (dashed line). Thus the NSGA-II is considered well converged.

3.3 Analysis of the optimization

The Pareto front on Figure 8(a) shows an important correlation between the objectives. The individual distribution of the Pareto front over h_{rib}/H, $e/2H$ and α is visible Figure 8(b). The clustering on the parameters space gives 6 centers and their performances are reported on Figure 8(a) as closed red symbols. CFD simulations were performed to qualify the metamodel interpolation on these centers. The performances of these re-converged points appear as open symbols on Figure 8(a) with the associated temperature variation fields. The difference between CFD-based and metamodel-based performances is from 0.6% to 8% for the effectiveness and from 8% to 15% for the total pressure drop. The difference is bigger for ΔP_{tot} due to difficulty of building an accurate metamodel for C_f because of the area of quasi null slope (see Section 3.1.). Looking at the parameters space, shapes associated to the center ◊ seem dubious and produce a discontinuity on the Pareto front. The CFD simulation confirms that the metamodel over estimates the Nusselt number for this center and therefore the effectiveness.

SOM on Figure 7 highlight the interdependences between the objectives and the parameters. As shown, a majority of individuals of the Pareto front have a rib height maximal.

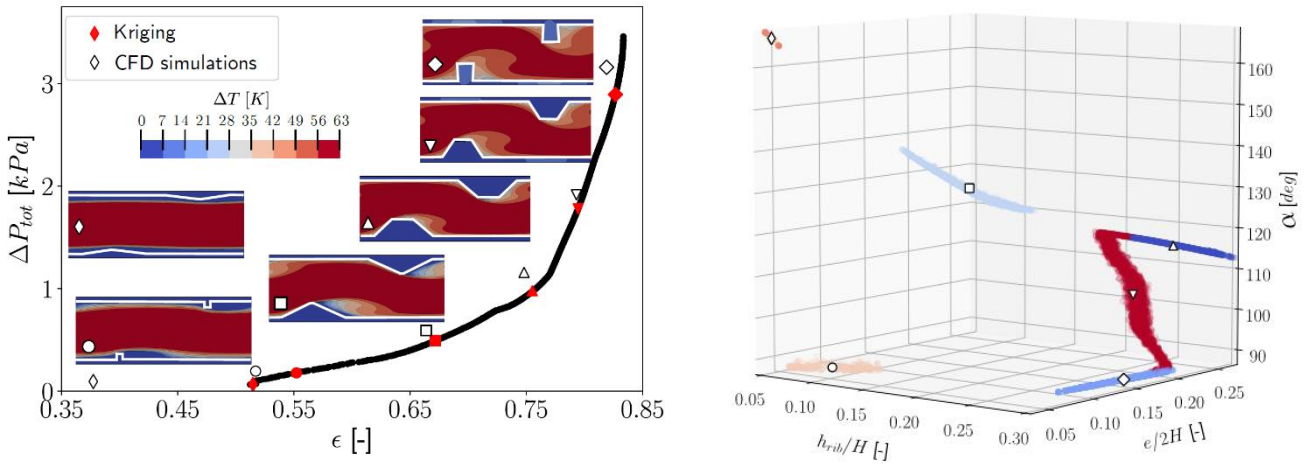

(a) (b)

Figure 8: **Optimization results – (a) The Pareto front and clusters centers achieved using the method. The closed red symbols represent the cluster center performances predicted by the metamodel. The open symbols are the cluster centers performances calculated from CFD simulations and the temperature variations are superimposed. – (b) Population distribution on D colored by clusters. Open symbols are the centers.**

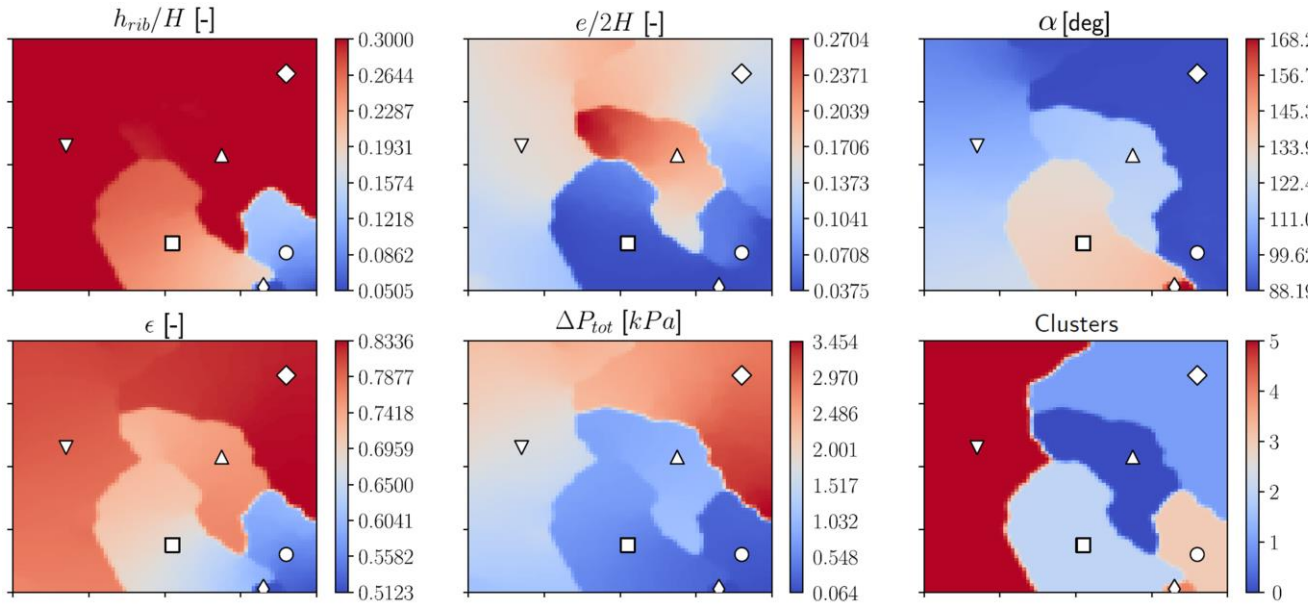

Figure 7: **Self-Organizing Maps of the Pareto front individuals: the three parameters (top), the two objectives and the clusters (bottom). The clusters centers are represented as open symbols.**

This leads to an important recirculation area behind the rib which increases Nu and C_f and therefore ε and ΔP_{tot}. When α increases (from ◇ to ▽) the pressure losses decrease. The recirculation area is less important such as the temperature homogenization. Thus the Nusselt number and effectiveness decrease. When the rib height is smaller and for significant α (◊ and ○), the temperature stratification deteriorates the heat transfer. Triangular and trapezoidal shapes (□, ▽ and △) may be an interesting compromise, particularly the △ one. In fact, after this point, there is a change on the Pareto front slope, leading to a rapid increase of the pressure losses for a slightly effectiveness improvement. These results highlight the major influence of the rib height h_{rib} on the heat transfer and pressure drop as reported by Kim et al. [4].

CONCLUSION

The multi-objective shape optimization of a CPHX was studied. The CPHX performances ε and ΔP_{tot} are calculated by coupling a NUT method to CFD calculations through the use of metamodels. There are based on kriging with adaptive sampling. Infill criteria are the maximum mean square error and the multi-points expected improvement. NSGA-II is then used to find the Pareto Front.

The metamodel convergence is analyzed through the evolution of the infill criteria stopping condition. Results show a limit of using expected improvement for C_f. Using the *IMSE* criterion instead of the *MMSE* one may improve the global metamodel accuracy with less observations.

The individuals clustering and the SOM highlight a finite number of optimal shapes, which are representative of the entire population. Some shapes are not interesting from the thermal point of view and may be penalized during the GA process.

NOMENCLATURE

Roman symbols

C	heat capacity flow rate	$\in \mathbb{R}$	$[W.K^{-1}]$
C^*	heat capacity ratio	$\in \mathbb{R}$	$[-]$
C_f	head loss coefficient	$\in \mathbb{R}$	$[-]$
C_{f0}	head loss coefficient, Blasius	$\in \mathbb{R}$	$[-]$
Cov	process covariance	$\in \mathbb{R}$	
c_p	specific heat	$\in \mathbb{R}$	$[J.kg^{-1}.K^{-1}]$
$\mathcal{D}$	parameters space	$\subset \mathbb{R}^3$	
$\mathcal{D}_e$	extended parameters space	$\subset \mathbb{R}^4$	
$\boldsymbol{D}$	experimental matrix	$\in \mathbb{R}^{n_o \times n_p}$	
$\boldsymbol{d}$	vector of basis functions	$\in \mathbb{R}^{n_p}$	
D_H	hydraulic diameter	$\in \mathbb{R}$	$[mm]$
$d_i(.)$	linear trend functions	$D_e \to \mathbb{R}$	
E	rib base width	$\in \mathbb{R}$	$[mm]$
e	rib top width	$\in \mathbb{R}$	$[mm]$
$\mathcal{F}$	objectives space	$\subset \mathbb{R}^2$	
H	canal height	$\in \mathbb{R}$	$[mm]$
H_E	heat exchanger height	$\in \mathbb{R}$	$[m]$
h_{rib}	rib height	$\in \mathbb{R}$	$[mm]$
I	Bessel function		
K	overall heat transfer coefficient	$\in \mathbb{R}$	$[K.m^2W^{-1}]$
L	rib-pitch	$\in \mathbb{R}$	$[mm]$
L_E	heat exchanger length	$\in \mathbb{R}$	$[m]$
Ln	likelihood function		
$\dot{m}$	mass flow rate	$\in \mathbb{R}$	$[kg.s^{-1}]$
m_K	kriging mean	$\in \mathbb{R}$	
$N_\square$	number of $\square$	$\in \mathbb{N}$	$[-]$
NTU	number of transfer units	$\in \mathbb{R}$	$[-]$
Nu	Nusselt number	$\in \mathbb{R}$	$[-]$
Nu_0	Nusselt number Dittus-Boelter	$\in \mathbb{R}$	$[-]$
n_o	number of observations	$\in \mathbb{N}$	$[-]$
n_p	number of linear functions	$\in \mathbb{N}$	$[-]$
$\boldsymbol{P}$	set of vector of parameters	$\in \mathcal{D}_e^{n_o}$	
P	pressure	$\in \mathbb{R}$	$[kPa]$
Pr	Prandtl number	$\in \mathbb{R}$	$[-]$
$\boldsymbol{p}$	vector of parameters	$\in \mathcal{D}_e$	
Q	total heat flux	$\in \mathbb{R}$	$[W]$
$\dot{q}$	heat flux density	$\in \mathbb{R}$	$[W.m^{-2}]$
q	number of new observations	$\in \mathbb{N}$	$[-]$
$\boldsymbol{r}(\boldsymbol{p})$	vector of covariance	$\in \mathbb{R}^{n_o}$	
$\boldsymbol{R}$	covariance matrix	$\in \mathbb{R}^{n_o \times n_o}$	
$R(.)$	spatial correlation function	${\mathcal{D}_e}^2 \to \mathbb{R}$	
REI	stopping condition for *q-EI*	$\in \mathbb{R}$	
RSD	stopping condition for *MMSE*	$\in \mathbb{R}$	
Re_{D_H}	Reynolds number	$\in \mathbb{R}$	$[-]$
S_{tot}	total heat transfer surface	$\in \mathbb{R}$	$[m^2]$
s_K^2	mean square error	$\in \mathbb{R}$	
T	temperature	$\in \mathbb{R}$	$[K]$
U_{deb}	bulk velocity	$\in \mathbb{R}$	$[m.s^{-1}]$
W_E	heat exchanger width	$\in \mathbb{R}$	$[m]$
$\boldsymbol{Y}$	set of known observations	$\in \mathbb{R}^{n_o}$	
Y	random variable	$\in \mathbb{R}$	
$y(.)$	realization of the random variable	$\in \mathcal{F}$	
Z	random process		

Greek symbols

α	rib angle	$\in \mathbb{R}$	$[deg]$
$\boldsymbol{\beta}$	vector of estimates of β	$\in \mathbb{R}^{n_p}$	
β	weights	$\in \mathbb{R}$	
ΔP_{tot}	total pressure drop	$\in \mathbb{R}$	$[kPa]$
δ_{EI}	relative tolerance for *q-EI*	$\in \mathbb{R}$	
δ_{SD}	relative tolerance for *MMSE*	$\in \mathbb{R}$	
ε	effectiveness	$\in \mathbb{R}$	$[-]$
λ	conductivity	$\in \mathbb{R}$	$[W.m^{-1}.K^{-1}]$
μ	viscosity	$\in \mathbb{R}$	$[Pa.s]$
ρ	density	$\in \mathbb{R}$	$[kg.m^{-3}]$
σ^2	process variance	$\in \mathbb{R}$	
$\boldsymbol{\theta}$	vector of characteristic lengths	$\in \mathbb{R}^4$	
θ	characteristic lengths	$\in \mathbb{R}$	

Subscript and Superscript

(i)	i[th] vector of parameters
(new)	new set of vector of parameters
a	air
in	inlet
out	outlet
ref	reference
w	water
$wall$	at the wall

Others

$\square^{-1}$	inverse operator
$\square^T$	transpose operator
$\mathbb{E}[.]$	mathematical expectation

REFERENCES

[1] Thulukkanam K. Heat exchanger design handbook. CRC Press; 2013.

[2] Wang L, Sunden B B. Experimental investigation of local heat transfer in a square duct with various-shaped ribs. Heat Mass Transf 2007;43:759.

[3] Rau G, Cakan M, Moeller D, Arts T. The Effect of Periodic Ribs on the Local Aerodynamic and Heat Transfer Performance of a Straight Cooling Channel. J Turbomach 1998;120:368–375.

[4] Kim KM, Kim BS, Lee DH, Moon H, Cho HH. Optimal design of transverse ribs in tubes for thermal performance enhancement. Energy 2010;35:2400–2406.

[5] Selbas R, Kızılkan Ö, Reppich M. A new design approach for shell-and-tube heat exchangers using genetic algorithms from economic point of view. Chem Eng Process Process Intensif 2006;45:268–75. doi:https://doi.org/10.1016/j.cep.2005.07.004.

[6] Guo J, Cheng L, Xu M. Multi-objective optimization of heat exchanger design by entropy generation minimization. J Heat Transf 2010;132:081801.

[7] Sanaye S, Hajabdollahi H. Multi-objective optimization of shell and tube heat exchangers. Appl Therm Eng 2010;30:1937–45. doi:https://doi.org/10.1016/j.applthermaleng.2010.04.018.

[8] Foli K, Okabe T, Olhofer M, Jin Y, Sendhoff B. Optimization of micro heat exchanger: CFD, analytical approach and multi-objective evolutionary algorithms. Int J Heat Mass Transf 2006;49:1090–1099.

[9] Lee H, Saleh K, Hwang Y, Radermacher R. Optimization of novel heat exchanger design for the application to low temperature lift heat pump. Energy 2012;42:204–12. doi:https://doi.org/10.1016/j.energy.2012.03.068.

[10] Saleh K, Aute V, Radermacher R, Azarm S. Chevron plate heat exchanger optimization using efficient approximation-assisted multi-objective optimization techniques. HVACR Res 2013;19:788–799.

[11] Wen J, Yang H, Tong X, Li K, Wang S, Li Y. Optimization investigation on configuration parameters of serrated fin in plate-fin heat exchanger using genetic algorithm. Int J Therm Sci 2016;101:116–25. doi:https://doi.org/10.1016/j.ijthermalsci.2015.10.024.

[12] Liu C, Bu W, Xu D. Multi-objective shape optimization of a plate-fin heat exchanger using CFD and multi-objective genetic algorithm. Int J Heat Mass Transf 2017;111:65–82.

[13] Hajabdollahi H, Tahani M, Fard MS. CFD modeling and multi-objective optimization of compact heat exchanger using CAN method. Appl Therm Eng 2011;31:2597–2604.

[14] Yin H, Ooka R. Shape optimization of water-to-water plate-fin heat exchanger using computational fluid dynamics and genetic algorithm. Appl Therm Eng 2015;80:310–318.

[15] Simpson TW, Mauery TM, Korte JJ, Mistree F. Kriging models for global approximation in simulation-based multidisciplinary design optimization. AIAA J 2001;39:2233–2241.

[16] Sasena MJ, Papalambros P, Goovaerts P. Exploration of metamodeling sampling criteria for constrained global optimization. Eng Optim 2002;34:263–278.

[17] Ribaud M, Gillot F, Helbert C, Blanchet-Scalliet C, Vial C. Robustness criterion for the optimization scheme based on kriging metamodel. 23ème Congrès Fr. Mécanique, 2017.

[18] Liu J, Song W-P, Han Z-H, Zhang Y. Efficient aerodynamic shape optimization of transonic wings using a parallel infilling strategy and surrogate models. Struct Multidiscip Optim 2017;55:925–943.

[19] EDF R&D, Code_Saturne version 5-1. n.d.

[20] Billard F, Laurence D. A robust k- $\varepsilon - \vd$/k elliptic blending turbulence model applied to near-wall, separated and buoyant flows. Int J Heat Fluid Flow 2012;33:45–58.

[21] Keshmiri A, Osman K, Benhamadouche S, Shokri N. Assessment of advanced RANS models against large eddy simulation and experimental data in the investigation of ribbed passages with passive heat transfer. Numer Heat Tr B-Fund 2016:1–15.

[22] Soulat L, Ferrand P, Moreau S, Aubert S, Buisson M. Efficient optimisation procedure for design problems in fluid mechanics. Comput Fluids 2013;82:73–86. doi:https://doi.org/10.1016/j.compfluid.2013.04.009.

[23] Deb K, Pratap A, Agarwal S, Meyarivan T. A fast and elitist multiobjective genetic algorithm: NSGA-II. IEEE Trans Evol Comput 2002;6:182–197.

[24] Buisson M, Ferrand P, Soulat L, Aubert S, Moreau S, Rambeau C, et al. Optimal design of an automotive fan using the Turb'Opty meta-model. Comput Fluids 2013;80:207–213.

[25] Sacks J, Welch WJ, Mitchell TJ, Wynn HP. Design and analysis of computer experiments. Stat Sci 1989:409–423.

[26] Roustant O, Ginsbourger D, Deville Y. DiceKriging, DiceOptim: Two R Packages for the Analysis of Computer Experiments by Kriging-Based Metamodeling and Optimization. J Stat Softw 2012;51:1–55.

[27] Martínez-Frutos J, Herrero-Pérez D. Kriging-based infill sampling criterion for constraint handling in multi-objective optimization. J Glob Optim 2016;64:97–115.

[28] Ginsbourger D, Le Riche R, Carraro L. Kriging is well-suited to parallelize optimization. Comput. Intell. Expens. Optim. Probl., Springer; 2010, p. 131–162.

[29] Damblin G, Couplet M, Iooss B. Numerical studies of space-filling designs: optimization of Latin Hypercube Samples and subprojection properties. J Simul 2013;7:276–289.

[30] Huang D, Allen TT, Notz WI, Zeng N. Global Optimization of Stochastic Black-Box Systems via Sequential Kriging Meta-Models. J Glob Optim 2006;34:441–466. doi:10.1007/s10898-005-2454-3.

[31] Lee S-M, Kim K-Y. Optimization of zigzag flow channels of a printed circuit heat exchanger for nuclear power plant application. J Nucl Sci Technol 2012;49:343–351.

[32] Bishop C. Pattern Recognition and Machine Learning. Springer New York; 2006.

[33] Picheny V, Ginsbourger D, Roustant O, Haftka RT, Kim N-H. Adaptive designs of experiments for accurate approximation of a target region. J Mech Des 2010;132:071008.